REPORT DOCUMENTATION PAGE

Form Approved
OMB No. 0704-0188

1. REPORT DATE *(DD-MM-YYYY)*	2. REPORT TYPE	3. DATES COVERED *(From - To)*
14-01-2016	Project Final Report	1 May 2012 - 30 September 2015

4. TITLE AND SUBTITLE
TOWARD SEAMLESS WEATHER-CLIMATE PREDICTION WITH A GLOBAL CLOUD RESOLVING MODEL

5a. CONTRACT NUMBER

5b. GRANT NUMBER
N000141210450

5c. PROGRAM ELEMENT NUMBER
ONR Marine Meteorology Program

6. AUTHOR(S)
Tim Li

5d. PROJECT NUMBER

5e. TASK NUMBER

5f. WORK UNIT NUMBER

7. PERFORMING ORGANIZATION NAME(S) AND ADDRESS(ES)
University of Hawaii
Office of Research Service
2440 Campus Road, Box 368
Honolulu, HI 96822

8. PERFORMING ORGANIZATION REPORT NUMBER

9. SPONSORING/MONITORING AGENCY NAME(S) AND ADDRESS(ES)
Office of Naval Research
875 North Randolph Street
Arlington, VA 22203-1995

10. SPONSOR/MONITOR'S ACRONYM(S)
ONR

11. SPONSOR/MONITOR'S REPORT NUMBER(S)

12. DISTRIBUTION/AVAILABILITY STATEMENT
DISTRIBUTION STATEMENT A: Distribution approved for public release; distribution is unlimited.

13. SUPPLEMENTARY NOTES

14. ABSTRACT

15. SUBJECT TERMS

16. SECURITY CLASSIFICATION OF:			17. LIMITATION OF ABSTRACT	18. NUMBER OF PAGES	19a. NAME OF RESPONSIBLE PERSON
a. REPORT	b. ABSTRACT	c. THIS PAGE			Tim Li
					19b. TELEPHONE NUMBER *(Include area code)* 808-956-9427

TOWARD SEAMLESS WEATHER-CLIMATE PREDICTION WITH A GLOBAL CLOUD RESOLVING MODEL

PI: Tim Li
IPRC/SOEST, University of Hawaii at Manoa
1680 East-West Road, POST Building 409B
Honolulu, Hawaii 96822
Phone: (808) 956-9427, fax: (808) 956-9425, e-mail: timli@hawaii.edu

Co-PI: Dr. Shian-Jiann Lin
Geophysical Fluid Dynamics Laboratory, NOAA
Princeton, New Jersey 08542
Tel: (609) 452-6514, Email: Shian-Jiann.Lin@noaa.gov

Co-PI: Melinda S. Peng
Naval Research Laboratory
Monterey CA 93943-5502
Phone: (831) 656-4704, fax: (831) 656-4769, e-mail: melinda.peng@nrlmry.navy.mil

Award Number: N000141210450
Project Period: April 2012 – Sept 2015

LONG-TERM GOAL

The long-term goal of this project is to developing a seamless weather and climate prediction system that has capability to predict accurately both weather phenomena such as tropical cyclones (TC) and other extreme weather events and longer climate-scale phenomena such as the Madden-Julian Oscillation (MJO) and the El Nino-Southern Oscillation (ENSO). Organized moist convections in the tropical atmosphere have their origins at space scale of less than 10 km, and they play a key role in the initiation and maintenance of mesoscale weather events such as super cloud clusters and large-scale phenomena such as MJO. The Navy is in urgent need to develop such a global high resolution model that has a proper dynamic core and physics packages and is capable of representing realistically convection and clouds across a wide range of spatial and temporal scales and suitable for prediction of extreme events in regional and global scales.

OBJECTIVE

We aim to develop a new global model framework with the goal of reducing the uncertainty in moist convective processes. The Geophysical Fluid Dynamics Laboratory (GFDL) High-Resolution Atmospheric Model (HiRAM) is proposed as a base framework for the next generation Navy global cloud resolving system. The HiRAM has a highly scalable finite volume dynamic core formulated on a cubed sphere. It is a non-hydrostatic, "cloud-resolving capable" global model designed to be applicable for a wide range of horizontal resolution from 100 km to 1 km. The objective of this project is to systematically evaluate the model's performance in weather (short and extended range) and climate (seasonal) predictions and provide a basis for the construction of next-generation Navy global cloud-resolving atmospheric forecast system suitable for operational requirements. We will in particular demonstrate the capability of this model in reproducing both short-range weather events such as mid-latitude synoptic systems and TCs and long-range climate variability such as MJO and ENSO teleconnection.

APPROACH

We proposed to conduct the following three sets of experiments using HiRAM:

Weather forecast experiment. The first experiment is daily 10-day forecasts at the 25-km for a continuous period of one years, starting from spring of 2012. The 12.5-km resolution can be done for shorter period (for example, at hurricane season) pending on the availability of computing resources at GFDL. This experiment is designed to evaluate the model performance in the conventional "weather forecast mode". A systematic evaluation of the model short-range weather forecast capability will be conducted and results will be compared with current operational models such as the Navy NOGAPS/NAVGEM and NCEP GFS. A special attention will be to the forecast skill of TC track and intensity and winter mid-latitude synoptic-scale systems.

AMIP-type experiment. The second is an AMIP-type experiment. The model is run for 20 years (1990-2010) with monthly or weekly observed SST as a lower boundary condition. The inclusion of a longer period is needed in order to examine the model's performance in reproducing the atmospheric internal modes such as MJO and teleconnection patterns associated with El Nino. This experiment may be identified as a "free run mode". A 25 km or a 12.5 km resolution will be used for the AMIP run. The capability of reproducing the observed MJO and ENSO variability in the "free run mode" is crucial for extended-range weather forecast. It has been shown that TC and

other synoptic wave activity are to a large extent controlled by low-frequency oscillations such as MJO and ENSO (Liebermann et al. 1994, Sobel and Maloney 2000, Fu et al. 2007, Hsu and Li 2011). Only when a model can capture realistic MJO structure and evolution in a free run, can this model predict the growth, propagation and phase transition of a real-case MJO event (otherwise the initial MJO signals would damp quickly with time).

Seasonal prediction experiment. The third is a seasonal prediction experiment similar to our TC forecast experiment. This may be termed as a "seasonal prediction mode". Such type of experiment is one step further toward achieving the goal of seamless weather-climate forecast. Through the evaluation of the model's seasonal forecast skill with forecasted SST (in which SST is determined based on the climatologic annual cycle plus a SST anomaly frozen at forecast initialization date), we will examine the model's practical predictability in extended range weather and seasonal climate prediction. The model's systematic bias in reproducing the seasonal mean state will be first examined, followed by the bias analysis in seasonal anomalies. The signal to noise ratio will be examined through multi-ensemble experiments. In addition to examining seasonal TC forecast skills in various basins, we will also examine the forecast skills in regional climate systems including the Asian monsoon, mid-latitude storm track, and the Pacific-North America pattern. The seasonal forecast experiments will be carried out for each season, in order to reveal the seasonal dependence of the model forecast capability.

We proposed to diagnose the experiments above, evaluate the model performance and assess the model forecast skills. Conventional diagnostic methods adopted at current operational centers are used to evaluate the model short-range weather forecast capability. Other diagnosis matrices such as the Wheeler-Hendon RMM based anomaly correlation coefficient (ACC) index and the signal-noise ratio based predictability index are used to assess the model extended-range forecast skill. In addition, we proposed to evaluate the relationships between TC genesis and large-scale parameters in various basins (e.g., tropical North Atlantic, eastern North Pacific, and western North Pacific), and evaluate the model's performance in reproducing the MJO variability and the ENSO teleconnection patterns.

WORK COMPLETED

This project aims to evaluate systematically the GFDL High-Resolution Atmospheric Model (HiRAM) capability in capturing both high-impact weather (such as TC) events and low-frequency (MJO and ENSO) climate oscillations. During the project period, we

thoroughly analyze the model performance in ENSO teleconnection patterns, MJO variability and TC statistics. A new double-plume convective scheme was developed. The diagnosis of 40-yr coupled model simulation showed that the new scheme is able to simulate much improved climate mean state and MJO variability in the tropics. The new model was further used for extended-range forecasts of Hurricane Sandy (2012) and Super Typhoon Haiyan (2013). A 10-yr (2003-2113) hindcast experiment for assessing MJO skill in the model was also conducted. The diagnosis of the model hindcast experiment showed that the model has a MJO forecast skill of up to 27 days. This skill score is among top of the current operational models around the world.

In addition, we examined MJO propagation and initiation dynamics with observational and model data. The published works include the studies of propagating and non-propagating MJOs across the Maritime Continent, MJO initiation mechanisms over western Indian Ocean, and effect of MJO low-frequency circulation on sudden track change of tropical cyclones.

RESULTS

1. MJO and ENSO teleconnection patterns as revealed from HiRAM AMIP simulations

Figure 1 shows observed and simulated MJO spectrum along the equator. It is clear that the model is able to capture, to a large extent, the observed spectrums of MJO, convectively coupled Kelvin waves, Rossby waves and inertial-gravity waves in northern winter.

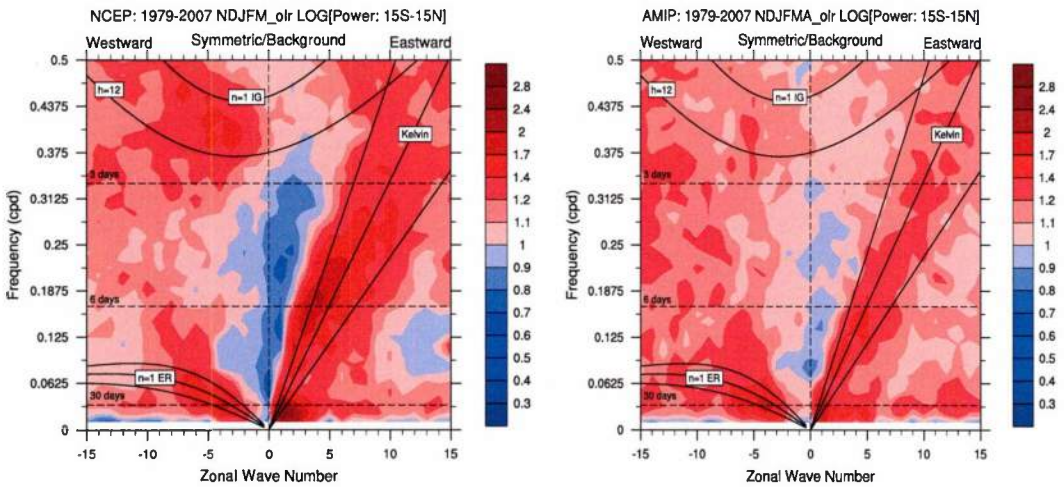

Fig. 1 Zonal wavenumber – frequency maps of power spectrum of observed (left) and

simulated (left) intraseasonal (20-80-day) OLR fields averaged between 15S and 15N in northern winter (NDJFM)

The MJO in the winter exhibits a pronounced eastward propagation along the equator (left panel of Fig. 2). Such a propagation characteristic is well captured by the HiRAM AMIP simulation (right panel of Fig. 2).

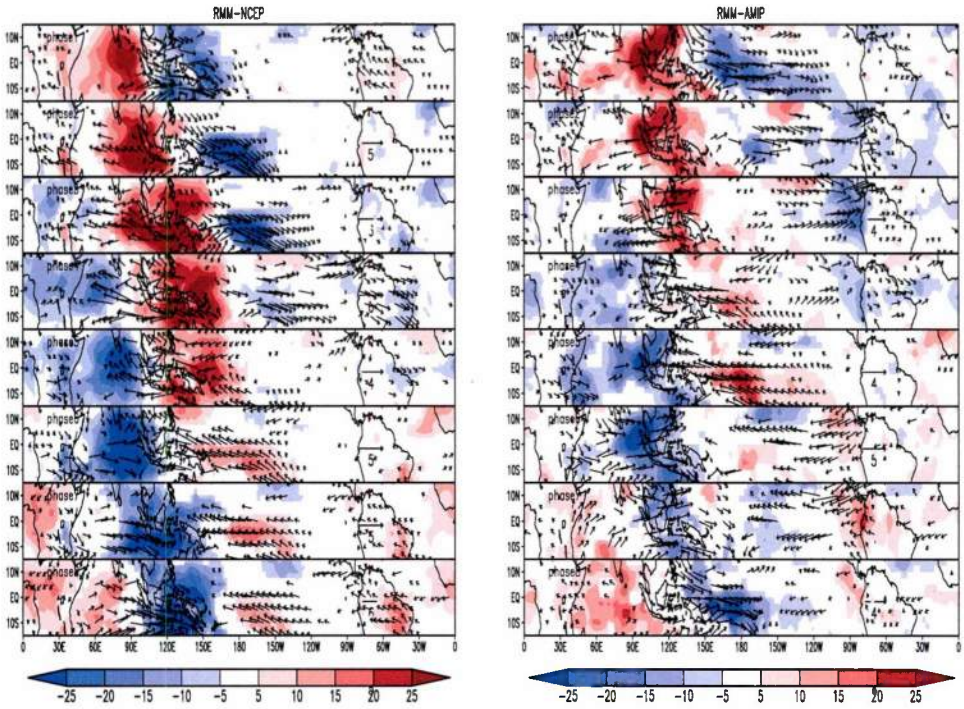

Fig. 2 RMM-based MJO phase-evolution maps in northern winter (left: observation, eight: simulation; shading: OLR, vector: 850hPa wind)

Different form northern winter, intraseasonal variability in boreal summer is dominated by northward propagation over the Asian monsoon region (such as Bay of Bengal and South China Sea). The top panel of Figure 3 shows the observed first two dominant EOF modes of rainfall structures associated with the boreal summer intraseasonal oscillation (ISO). While the maximum rainfall center in EOF1 is located in the equatorial eastern Indian Ocean, the dominant rainfall pattern in EOF2 exhibits a northwest-southeast tilted structure. Such rainfall patterns are well captured by the model.

In addition to the diagnosis of MJO variability, we also examined the model

performance in capturing remote and local circulation patterns associated with central Pacific and eastern Pacific El Ninos. We noted that the teleconnection patterns over the Asian monsoon and tropical Indian Ocean are well reproduced for both types of El Ninos. However, for the Pacific-North America (PNA) pattern, the model can only reproduce it during the mature winter of the eastern Pacific El Nino, and cannot during the central Pacific El Nino.

Currently we are aiming to improve the model deep convective scheme, to better reproduce the MJO and ENSO patterns.

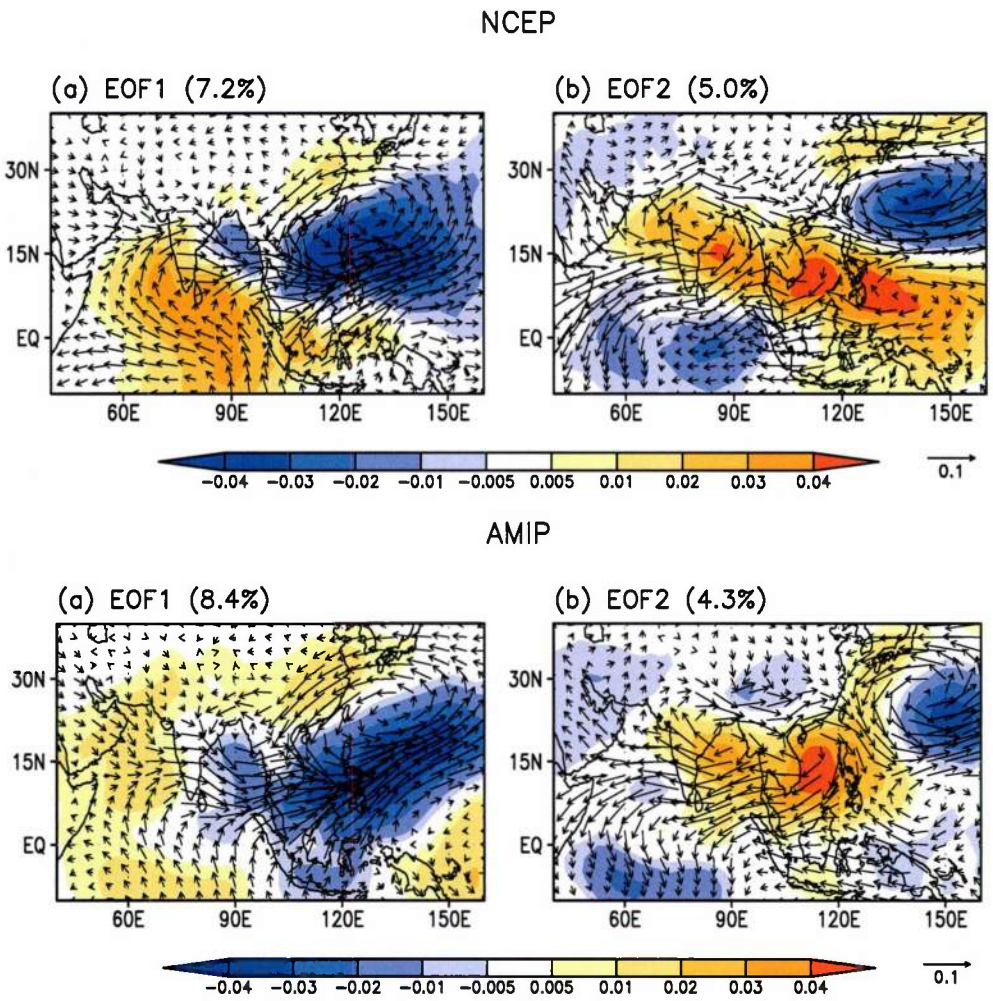

Fig. 3 Observed (top panel) and simulated (bottom panel) first two EOF patterns of the intraseasonal (20-80-day) rainfall field in boreal summer (MJJAS) over the tropical Indian Ocean-western Pacific warm pool region

2. Changes of MJO features under global warming

This study estimates MJO change under the A1B greenhouse gas emission scenario using the ECHAM5 AGCM whose coupled version (ECHAM5/MPI-OM) has simulated best MJO variance among fourteen CGCMs. The model has a horizontal resolution at T319 (about 40 km) and is forced by the monthly evolving SST derived from the ECHAM5/MPI-OM at a lower resolution of T63 (about 200 km). Two runs are carried out covering the last 21 years of the 20th and 21st centuries. The NCEP/NCAR Reanalysis products and observed precipitation are used to validate the simulated MJO during the 20th century, based on which the 21st century MJO change is compared and predicted.

The validation indicates that the previously reported MJO variances in the T63 coupled version are reproduced by the 40-km ECHAM5. More aspects of MJO, such as the eastward propagation, structure, and dominant frequency and zonal wavenumber in power spectrum, are simulated reasonably well. The magnitude in power, however, is still low so that the signal is marginally detectable and embedded in the over-reddened background.

Under the A1B scenario, the T63 ECHAM5/MPI-OM projected an over 3 K warmer tropical sea surface that forces the 40-km ECHAM to produce wetter tropics. The enhanced precipitation variance shows more spectral enhancement in background than in most wavebands. The zonal winds associated with MJO, however, are strengthened in the lower troposphere but weakened in the upper. On the one hand, the 850-hPa zonal wind has power nearly doubled in 30-60-day bands, demonstrating relatively clearer enhancement than the precipitation in MJO with the warming. A 1-tailed Student's t-test suggests that most of the MJO changes in variance and power spectra are statically significant. Subject to a 20-100-day band-pass filtering of that wind, an EOF analysis indicates that the two leading components in the 20th–century run have a close structure to but smaller percentage of explained-to-total variance than those in observations; the A1B warming slightly increases the explained percentage and alters the structure. An MJO index formed by the two leading principal components discloses nearly doubling in the number of prominent MJO events with a peak phase occurring in February and March. A composite MJO life cycle of these events favors the frictional moisture convergence mechanism in maintaining the MJO and the nonlinear wind-induced surface heat exchange (WISHE) mechanism also appears in the A1B warming case. On the other hand, the Slingo index based on the 300-hPa zonal wind discloses that the upper-level MJO tends to be suppressed by the A1B warming, although the loose relationship with ENSO remains unchanged. Possible cause for the different change of MJO in the lower and upper troposphere is discussed.

3. Projected future increase in Hawaiian tropical cyclones

Possible future changes in tropical cyclone (TC) activity around the Hawaiian Islands are investigated using the state-of-the-art climate models[1–3]. We find that the future experiments (2075–2099) project a consistent and robust increase in frequency of TC occurrence around the Hawaiian Islands by about 179% compared with the simulated present-day climate (1979–2003). We apply a statistical methodology[3] to address factors responsible for the increase in TC frequency. The results reveal that the TC track change is the major factor responsible for the increased TC frequency. This implies significant future changes in large-scale flows. We find that the large-scale westward steering flows indeed increased in the subtropical central to eastern Pacific, which acts as a "pathway" leading more TCs from farther eastern Pacific toward the Hawaiian Islands. The steering flow changes are robust regardless of models used and the assumed global warming scenarios. These results highlight possible future increase in storm-related socio-economic damage in the future in the Hawaiian Islands.

4. Changes to environmental parameters controlling TC genesis under global warming

This study uses the MRI high-resolution Atmospheric Climate Model to determine whether environmental parameters that control tropical cyclone (TC) genesis in the Western North Pacific (WNP) and North Atlantic (NA) may differ in the global warming state. A box difference index (BDI) was computed to quantitatively assess the role of environmental controlling parameters. The diagnosis of the model outputs shows that in the WNP, dynamical variables are of primary importance for separating developing and non-developing disturbances in the present-day climate, and such a relationship remains unchanged in a future warmer climate. This is in contrast to the NA, where BDI increases for all dynamic variables investigated while it shows little change for thermodynamic variables. This implies that, when compared with the present-day climate in which thermodynamic variables have a major control on TC genesis, dynamic and thermodynamic variables have equal control in the NA under the future warmer climate.

5. Improved MJO simulation in HiRAM due to new double plume convective parameterization scheme

The original version of HIRAM simulated well the mean climate when forced by observed SSTs. However, when coupled with an ocean GCM, it produced significant

cold/dry bias in the equatorial Pacific, negatively affecting ENSO simulation. To reduce the biases, a modified convection scheme was recently developed at GFDL. An additional plume was introduced to represent deep and organized convection with entrainment rate dependent on ambient RH.

This new scheme incorporates recent findings on key processes for modeling MJO convection (including shallow cumulus moistening ahead of deep organized convection, cold pools due to precipitation re-evaporation). The modified scheme is called a double plume (DP) scheme, which can significantly reduce the equatorial Pacific cold/dry bias, improve simulated precipitation and cloud response to ENSO, maintain competitive simulation of global TC statistics, and improve MJO simulation.

Figure 4 shows observed and simulated OLR power spectrum over the equatorial Indian Ocean. It is clear that the DP version model captures the observed amplitude of OLR variability on the intraseasonal time scale, compared to original "non-DP" version model. Both the coupled models were integrated for 40 years.

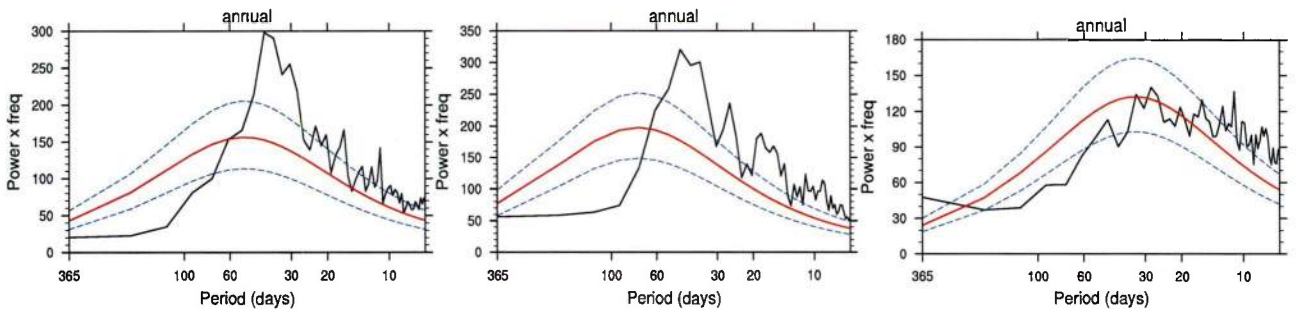

Fig. 4 The power spectrum of observed (left) and simulated ("DP" in middle and "non-DP" in right) intraseasonal (20-80-day) OLR fields averaged over (10S-10N, 60E-100E)

The MJO exhibits a pronounced eastward propagation along the equator (left panel of Fig. 5) in northern winter (from November to April). Such a propagation characteristic is better captured by the HiRAM DP version model (middle panel of Fig. 5) than its "non-DP" version model (right panel of Fig. 5).

The propagation difference may be clearly seen in the time-longitude section of lagged correlation between the intraseasonal precipitation anomaly in central equatorial Indian Ocean (90E, 0N) and precipitation and 850-hPa zonal wind fields along the equator (figure not shown).

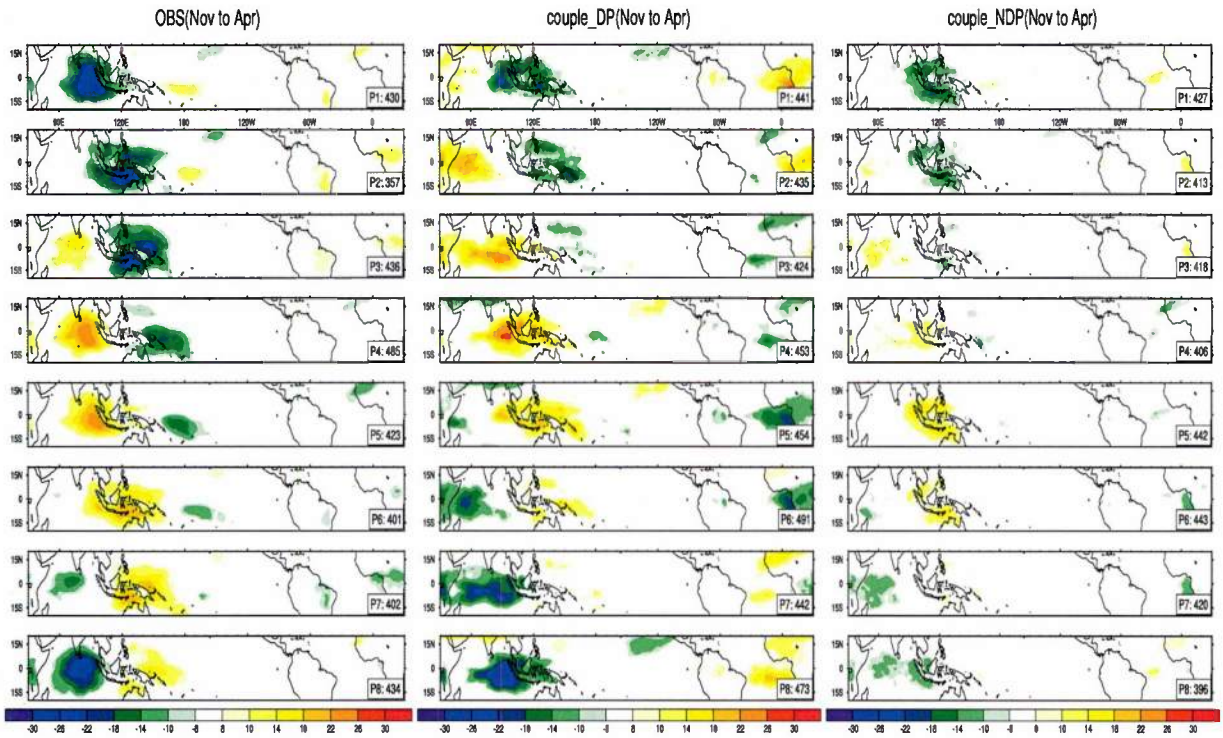

Fig. 5 RMM-based MJO phase-evolution maps of the OLR anomalies in northern winter (left: observation, middle: DP version model simulation, right: non-DP version model simulation)

5. Extended range tropical cyclone (TC) forecast experiments

The coupled version of HiRAM with use of the new DP convective parameterization scheme was used to conduct beyond weather time scale prediction of two high-impact TCs, Hurricane Sandy in 2012 and Super Typhoon Haiyan in 2013 (Xiang et al. 2014). The coupled model initial condition was derived based on a nudging scheme in which the model prognostic variables such as U, V, SLP, geopotential height, air temperature and SST were nudged toward NCEP final analysis (FNL) fields. There were 24 ensemble forecast members each day. TCs in the model were determined based on Lucas Harris's simply tracker. A 'correct' forecast is defined when TCs form during one day before and after the observed genesis (i.e., a 3-day window) within radius of 1100 km. A false alarm was counted when TCs form 5 days before and 5 days after the 'correct' prediction window within 1100 km radius of circle.

Figure 6 shows the forecast diagnosis results for both Sandy (2012) and Haiyan (2013). Note that the possibility of detection (POD) for both Sandy (2012) and Haiyan (2013) is above 70% for 5- to 11- day lead, while false alarm ratio is lower than 12%. The

numerical model results indicate that Sandy and Haiyan genesis is predictable at a lead time of 11 days.

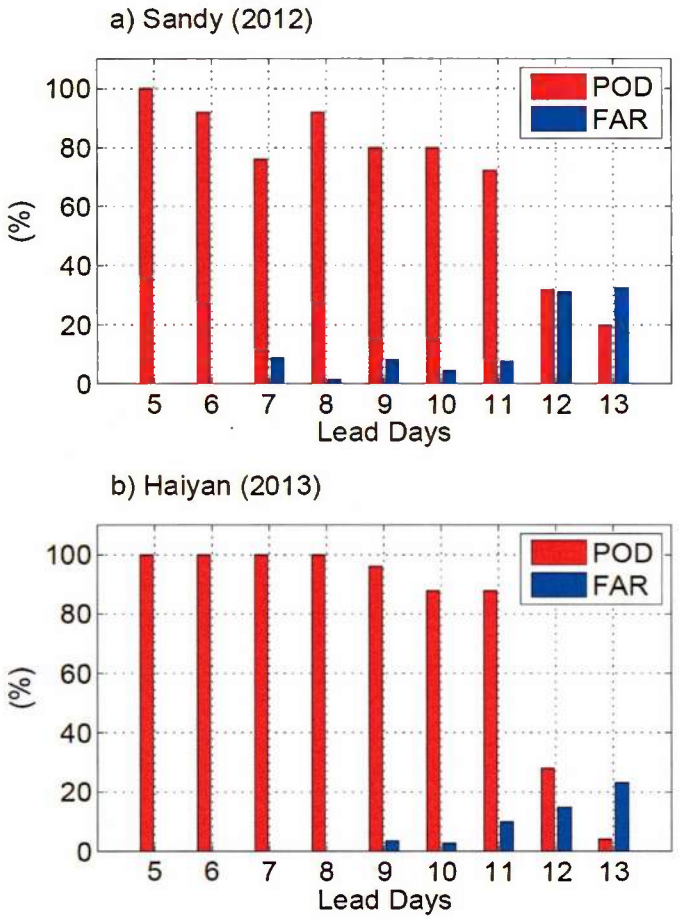

Fig. 6 Possibility of detection (POD, red) and false alarm ratio (FAR, blue) as a function of forecast lead days for Sandy (2012, top) and Haiyan (2013, bottom)

It is also found that landfall timing can be well predicted one week ahead for Sandy (2012) and two weeks ahead for Haiyan (2013).

The beyond weather time scale prediction is mainly attributed to the successful prediction of MJO and easterly waves in the tropical Atlantic and Pacific Oceans (figures not shown). The numerical results suggest that HiRAM has potential to bridge a gap between weather and climate scales.

6. Effects of Monsoon Trough Intraseasonal Oscillation on Tropical Cyclogenesis over the Western North Pacific

The effects of intraseasonal oscillation (ISO) of the western North Pacific (WNP) monsoon trough on tropical cyclone (TC) formation were investigated using the

Advanced Research Weather Research and Forecasting (WRF-ARW) model. A weak vortex was specified initially and inserted into the background fields containing climatologic mean anomalies associated with active and inactive phases of monsoon trough ISO.

The diagnosis of simulations showed that monsoon trough ISO can modulate TC development through both dynamic and thermodynamic processes. The dynamic impact is attributed to the lower-middle tropospheric large-scale vorticity associated with monsoon trough ISO. Interactions between a cyclonic vorticity in the lower-middle troposphere during the active ISO phase and a vortex lead to the generation of vortex-scale outflow at midlevel, which promotes the upward penetration of friction-induced ascending motion and thus upward moisture transport. In addition, the low-level convergence associated with active ISO also helps the upward moisture transport. Both processes contribute to stronger diabatic heating and thus promote a positive convection–circulation–moisture feedback. On the other hand, the large-scale flow associated with inactive ISO suppresses upward motion near the core by inducing the midlevel inflow and the divergence forcing within the boundary layer, both inhibiting TC development. The thermodynamic impact comes from greater background specific humidity associated with active ISO that allows a stronger diabatic heating. Experiments that separated the dynamic and thermodynamic impacts of the ISO showed that the thermodynamic anomaly from active ISO contributes more to TC development, while the dynamic anomalies from inactive ISO can inhibit vortex development completely.

7. Roles of Synoptic-scale Wave Train, Intraseasonal Oscillation and High-frequency Eddies in Genesis of Typhoon Manyi (2001)

Experiments using the WRF model were conducted to investigate the effects of multi-scale motions on the genesis of typhoon Manyi (2001) in the western North Pacific. The precursor signal associated with this typhoon genesis was identified as a northwest-southeast-oriented synoptic-scale wave train (SWT). The model successfully simulated the genesis of the typhoon in the wake of the SWT. Further experiments were conducted to isolate the effects of the SWT, the intraseasonal oscillation (ISO), and high frequency (shorter than 3 days) eddies in the typhoon formation.

Removing the SWT in the initial and boundary conditions eliminates the typhoon genesis. This points out the importance of the SWT in the typhoon genesis. It was noted that the SWT strengthened the wake cyclone through southeastward energy dispersion. The strengthening wake cyclone triggered multiple episodes of strong sustained

convective updrafts, leading to aggregation of vertical vorticity and formation of a self-amplified mesoscale core vortex through a 'bottom-up' development process. Removing the ISO flow eliminates the typhoon genesis, as the ISO significantly modulated the strength of the SWT through accumulation of wave activity. In the absence of SWT-ISO scale interaction, the southeastward energy dispersion was weakened significantly, thus the strengthening of the wake cyclone did not occur. As a result, the successive strong sustained convective updrafts disappeared. Removing the high frequency eddies did not eliminate the typhoon genesis but postponed the genesis for about 36 hour.

8. A 10-yr MJO hindcast experiment and diagnosis of the model output

The coupled version of HiRAM with use of the new DP convective parameterization scheme was used to conduct 10-yr (2003-2013) hindcast experiment (Xiang et al. 2015). The coupled model initial condition was derived based on a nudging scheme in which the model prognostic variables such as U, V, SLP, geopotential height, air temperature and SST were nudged toward NCEP final analysis (FNL) fields. The hindcast period is November to April. The model was run once every five days (i.e., 1st, 6th, 11th, 16th, 21st, and 26th each month). There were 6 ensemble forecast members each run (00Z, 04Z, 08Z, 12Z, 16Z, and 20Z). The model was integrated for 50 days for each ensemble.

Figure 7 shows the bi-variate Anomaly Correlation Coefficient (ACC) and Root Mean Square Error (RMSE) of the model MJO prediction during the 10-yr period. The ACC for individual member (grey lines in Fig. 7a) drops rapidly for the first 20 days and the 6 members' mean skill is about 19 days with the ACC exceeding 0.5. As expected, the ACC for the 6 members ensemble mean (red line in Fig. 7a) is superior to that from individual member with the skill reaching out to 25 days. This RMM skill is among top of current operational forecast models in the world.

In accordance with the decrease of the bivariate ACC, the RMSE increases rapidly during the first 20 days but keeps almost flat during the time range of 20-40 days (Fig. 7b). Using the same criterion of ACC in excess of 0.5, the prediction skills for RMM1 and RMM2 are estimated to be 28 and 22 days (not shown), respectively, suggesting that EOF1 is more predictable than EOF2 mode in this model forecast system. We also examine the prediction skill for individual variables. As expected, the prediction skill for OLR is lower (17 days) than the other two circulation variables U850 (24 days) and U200 (22 days).

Large contrasts are found for the MJO forecast skill between initially strong and weak cases (41 vs. 17 days), and also for target strong and weak cases (42 vs. 9 days). Meanwhile, the prediction skill is significantly higher during phases 2, 3, 4, and 5 compared to the other 4 phases, indicating that the propagation of wet anomalies is more predictable than the relatively dry anomalies. The amplitude and propagation speed are reasonably well predicted, ensuing the high prediction skill especially for initially strong cases.

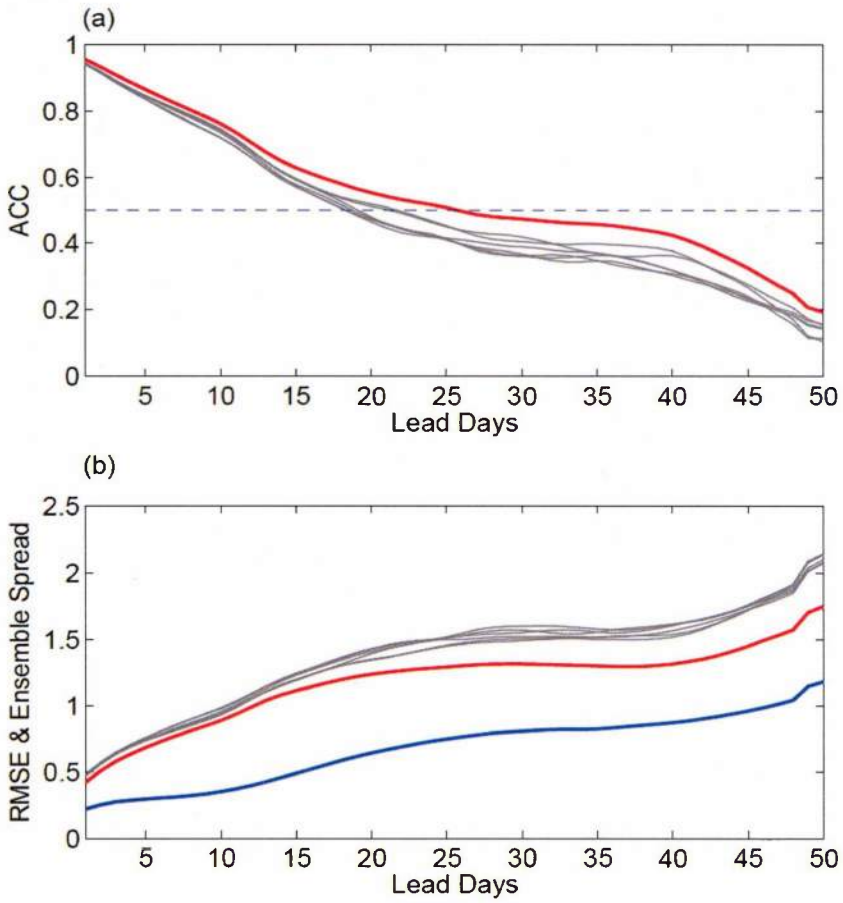

Figure 7 MJO prediction skill in boreal winter. (a) The bivariate ACC for individual member (grey) and 6 member ensemble mean (red) as a function of forecast lead days. (b) RMSE of individual member (grey) and ensemble mean (red), and the ensemble spread relative to the 6 member ensemble mean (blue).

9. Mechanisms for propagating and non-Propagating MJO Events across Maritime Continent

The observed outgoing longwave radiation and ERA-I data during 1979-2008 (from November to April) were analyzed to reveal fundamental differences between eastward-propagating (EP) and non-propagating (NP) MJO events across the maritime continent. It was found that when the maximum MJO convection arrives near 120°E, a positive moisture tendency lies in a longitudinal zone (130°E - 170°E, 10°S - 10°N) for the EP cases whereas a negative tendency appears in the same region for the NP cases. For the latter there are clearly detectable westward-propagating Rossby-wave-type dry signals over the equatorial central-western Pacific. A moisture budget analysis shows that the positive tendency of specific humidity in the EP composite is mainly attributed to the advection of the mean moisture by intraseasonal ascending motion anomaly, whereas the negative tendency in the NP composite arises from the advection of anomalous dry air by the mean easterly and the advection of the mean moisture by the anomalous easterly.

10. MJO initiation processes during DYNAMO period

During the DYNAMO campaign period, two strong MJO events occurred from middle of October to middle of December (referred to as MJO I and MJO II respectively). Both the events were initiated over the western equatorial Indian Ocean (WIO) around 50°-60°E. Using multiple observational data products (ERA-Interim, ECMWF final analysis and NASA MERRA), we unveil specific processes that triggered the MJO convection in the WIO. It is found that 10 days prior to MJO I initiation, a marked large-scale ascending motion anomaly appeared in the lower troposphere over the WIO. The cause of this intraseasonal vertical motion anomaly was attributed to anomalous warm advection by a cyclonic gyre anomaly over the northern IO. The MJO II initiation was preceded by a low-level specific humidity anomaly. This lower-tropospheric moistening was attributed to the advection of mean moisture by anomalous easterlies over the equatorial IO. It was found that upper-tropospheric circumnavigating signals did not contribute the initiation of both the MJO events. Thus the EOF-based RMM indices should not be used to determine MJO initiation time and location because they are primarily used to capture large scale eastward-propagation signals, not localized features.

11. A Spatial-Temporal Projection Model for Extended-Range Forecast in the Tropics

A spatial-temporal projection model (STPM) was constructed for the extended-range (10-30-day) forecast (ERF) of tropical outgoing longwave radiation anomalies (OLRA). A 10-yr hindcast result shows that, different from previous statistical models, the skill scores of the STPM dropped slowly with forecast lead times. Useful skills can be detected at 30-35 day leads over most tropical regions. The highest temporal correlation

coefficient (TCC) of 0.4-0.5 appears over the Maritime Continent (Indian and western North Pacific monsoon regions) in boreal winter (summer). The STPM is also able capable in predicting the spatial evolutions of convective anomaly, including the zonal and meridional propagation of OLRA. The forecast of the Real-time Multivariate MJO (RMM) indices shows that the STPM attains a higher skill than previous statistical models. The STPM shows comparable skills with the state-of-the-art dynamic models such as ECMWF during the DYNAMO campaign period.

12. Interactions between Typhoon Megi and a Low-frequency Monsoon Gyre

The WRF model is used to investigate the sharp northward turn of super typhoon Megi (2010) after it moved westward and crossed the Philippines. The NCEP analyzed fields during this period are separated into a slowly varying background flow component, a 10-60-day low frequency component representing the monsoon gyre, and a 10-day high-pass filtered component representing Megi and other synoptic-scale motion. It appears that the low-frequency (10-60-day) monsoon gyre interacted with Megi and affected its track. To investigate the effect of the low-frequency mode on Megi, numerical experiments were designed. In the control experiment, the total fields of the analysis are retained in the initial and boundary conditions, and the model is able to simulate Megi's sharp northward turn. In the second experiment, the 10-60-day monsoon gyre mode is removed from the initial and lateral boundary fields and Megi moves westward and slightly northwestward without turning north. Tracks of the relative positions between the Megi and the monsoon gyre centers suggest that a Fujiwhara effect may exist between the monsoon gyre and Megi. The northward turning of both Megi and the monsoon gyre occurred when the two centers are close to each other and the beta drift was enhanced.

13. Three Types of MJO Initiation Processes over the Western Indian Ocean

Thirty strong Madden–Julian Oscillation (MJO) events in boreal winter 1982–2001 are selected to investigate the triggering processes of MJO convection over the western equatorial Indian Ocean (IO). These MJO events are classified into three types, according to their dynamic and thermodynamic precursor signals in situ. In Type I, a remarkable increase in low-level moisture occurs, on average, 7 days prior to the convection initiation. This low-level moistening is mainly due to the advection of the background mean moisture by easterly wind anomalies over the equatorial IO. In Type II, lower-tropospheric ascending motion anomalies develop, on average, 4 days prior to the initiation. The cause of this ascending motion anomaly is attributed to the anomalous warm advection, set up by a suppressed MJO phase in the equatorial IO. In Type III, there are no clear dynamic and thermodynamic precursor signals in situ. The

convection might be triggered by energy accumulation in the upper layer associated with Rossby wave activity fluxes originated from the mid-latitudes.

IMPACT/APPLICATIONS

The current effort may lead to the improved understanding of MJO dynamics and the development of next generation navy operational weather-climate prediction model.

TRANSITIONS

Results from this study may lead to the development of a base model for next-generation navy operational seamless weather-climate forecast system. The model dynamic core and physics package may be transitioned into NRL as a 6.4 project.

RELATED PROJECTS

This project is complementary to our NSF funding entitled "Upscale feedback of tropical atmospheric synoptic-scale variability to intra-seasonal oscillation" in which we are investigating two-way interactions between the synoptic-scale motion (including TC) and MJO.

PUBLICATIONS

The following are papers published during 2013-2015 that are fully or partially supported by this ONR grant:

1. Bi, M., T. Li, M. Peng, and X.-Y. Shen, 2015: Interactions between Typhoon Megi (2010) and a Low-frequency Monsoon Gyre. J. Atmos. Sci., 72 (7), 2682-2702.
2. Bi, M., T. Li, X. Shen, and M. Peng, 2015: To What Extent the Presence of Real-Strength Tropical Cyclones Influences the Estimation of Atmospheric Intraseasonal Oscillation Intensity? Atmospheric Science Letters, in press
3. Cao, X., T. Li, M. Peng, W. Chen, and G. Chen, 2014: Effects of the monsoon trough interannual variation on tropical cyclogenesis over the western North Pacific. *GRL*, 41 (12), 4332-4339, doi:10.1002/2014GL060307

4. Cao, X., T. Li, M. Peng, W. Chen, and G. Chen, 2014: Effects of monsoon trough intraseasonal oscillation on tropical cyclogenesis in the western North Pacific. *J. Atmos. Sci.*, 71, 4639-4660.
5. Chen L. T. Li, Y. Yu, 2015: Causes of Strengthening and Weakening of ENSO Amplitude under Global Warming in Four CMIP5 Models, J. Climate, 28 (8), 3250-3274.
6. Chung, P.-H., and T. Li, 2015: Characteristics of tropical cyclone genesis in the western North Pacific during the developing and decaying phases of two types of El Niño. Journal of Tropical Meteorology, 21 (1), 14-22.
7. Feng, J., T. Li, and W. Zhu, 2015: Propagating and Non-Propagating MJO Events over Maritime Continent, J. Climate, in press.
8. Hsu, P.-C., T. Li, L. You, J. Gao, and H. Ren: A spatial-temporal projection model for 10-30 day rainfall forecast in South China. *Clim. Dyn.*, in press.
9. Li, C.-Y., W. Zhou, and T. Li, 2014: Influences of the Pacific-Japan teleconnection pattern on synoptic-scale variability in the western North Pacific. *J. Climate*, 140-154.
10. Li, T., 2014: Recent advance in understanding the dynamics of the Madden-Julian Oscillation, *J. Meteor. Res.*, 28, 1-33.
11. Li, T., L. Zhang, and H. Murakami, 2015: Strengthening of the Walker Circulation under Global Warming in an Aqua-Planet General Circulation Model Simulation, Adv. Atmos. Sci., in press.
12. Li, T., C. Zhao, P.-C. Hsu, and T. Nasuno, 2015: MJO Initiation Processes over the Tropical Indian Ocean during DYNAMO/CINDY2011. J. Climate, 28 (6), 2121-2135.
13. Liu, P., T. Li, B. Wang, M. Zhang, J.-J. Luo, Y. Masumoto, X. Wang, and E. Roekner, 2013: MJO change with A1B global warming estimated by the 40-km ECHAM5. *Clim. Dyn.*, **41** (3-4), 1009-1023, doi:10.1007/s00382-012-1532-8.
14. Mei, S., T. Li, and W. Chen, 2015: Three Types of MJO Initiation Processes over the Western Equatorial Indian Ocean, Advances in Atmospheric Sciences, in press.
15. Murakami, H., B. Wang, T. Li, and A. Kitoh, 2013: Projected future increase in tropical cyclones near Hawaii. *Nature Climate Change*, **3**, 749-754, doi:10.1038/nclimate1890.
16. Murakami, H., T. Li, and M. Peng, 2013: Changes to Environmental Parameters that Control Tropical Cyclone Genesis under Global Warming. *GRL*, **40** (10), 2265-2270, doi:10.1002/grl.50393.
17. Murakami, H., Tim Li, and Pang-chi Hsu, 2014: Contributing factors to the recent high level of Accumulated Cyclone Energy (ACE) and Power Dissipation Index (PDI) in the North Atlantic. *J. Climate*, 27 (8), 3023-3034.

18. Nasuno, T., T. Li, and K. Kikuchi, 2015: Moistening processes before the convective initiation of Madden-Julian Oscillation events during the CINDY2011/DYNAMO period. Mon. Wea. Rev., 143 (2), 622-643.
19. Wang, L., T. Li, and T. Zhou, 2015: Effect of high-frequency wind on intraseasonal SST variabilities over the mid-latitude North Pacific region during boreal summer, Climate Dynamics, (DOI) 10.1007/s00382-015-2496-2
20. Xiang, B., S.-J. Lin, M. Zhao, S. Zhang, G. Vecchi, T. Li, X. Jiang, L. Harris, J.-H. Chen, 2015: Beyond weather time scale prediction for Hurricane Sandy and Super Typhoon Haiyan in a global climate model, Monthly Weather Review, 143, 524-535.
21. Xiang, B., M. Zhao, X. Jiang, S.-J. Lin, T. Li, X. Fu, and G. Vecchi, 2015: 3-4 week MJO prediction skill in a GFDL Coupled Model, J. Climate, in press.
22. Xu, Y., T. Li, and M. Peng, 2014: Roles of synoptic-scale wave train, intraseasonal oscillation, and high-frequency eddies in genesis of Typhoon Manyi (2001). *J. Atmos. Sci.*, 71, 3706–3722.
23. Yang, Y., T. Li, W. Yu, K. Li, 2015: What Controls Seasonal Variations of the Diurnal Cycle of Sea Surface Temperature in the Eastern Tropical Indian Ocean? J. Climate, in press.
24. Yu, J.-H., T. Li, Z. Tan, and Z. Zhu, 2015: Effects of tropical North Atlantic SST on tropical cyclone genesis in the western North Pacific. Climate Dynamics, in press.
25. Yuan, J., T. Li, and D. Wang, 2015: Precursor synoptic-scale disturbances associated with tropical cyclogenesis in the South China Sea during 2000-2011, International Journal of Climatology, in press.
26. Zhu, Z.-W., T. Li, P.-C. Hsu, and J.-H. He, 2015: A Spatial-Temporal Projection Model for Extended-Range Forecast in the Tropics, Clim. Dyn., 45, 1085-1098.